Linear electro-optical behavior of hybrid nanocomposites based on silicon carbide nanocrystals and polymer matrices

J. Bouclé,[1,2,*] A. Kassiba,[1,*] M. Makowska-Janusik,[3] N. Herlin-Boime,[2] C. Reynaud,[2] A. Desert,[1] J. Emery,[1] A. Bulou,[1] J. Sanetra,[4] A. A. Pud,[5] and S. Kodjikian[6]

[1]*Institut de Recherche en Ingénierie Moléculaire et Matériaux Fonctionnels FR CNRS 2575 – Laboratoire de Physique de l'Etat Condensé, UMR CNRS 6087, Université du Maine, 72085 Le Mans Cedex 9, France*

[2]*Laboratoire Francis Perrin – Service des Photons, Atomes et Molécules, CEA-CNRS URA 2453- CEA/DSM de Saclay, 91191 Gif sur Yvette Cedex, France*

[3]*Institute of Physics, Akademia Im.Jana Dlugosza, Al.Armii.Krajowej, 42-200 Czestochowa, Poland*

[4]*Institute of Physics, Krakow University of Technology, Ul.Podchorazych, 30-084 Krakow, Poland*

[5]*Institute of Bioorganic Chemistry and Petrochemistry, National Academy of Sciences of Ukraine, 50 Kharkovskoye Shosse, 02160 Kiev, Ukraine*

[6]*Institut de Recherche en Ingénierie Moléculaire et Matériaux Fonctionnels FR CNRS 2575 – Laboratoire des Oxydes et des Fluorures, UMR CNRS 6010, Université du Maine, 72085 Le Mans Cedex 9, France*

(Received 21 February 2006; revised manuscript received 21 July 2006; published 15 November 2006)

An electro-optical activity has been recently reported for hybrid nanocomposite thin films where inorganic silicon carbide nanocrystals (ncSiC) are incorporated into polymer matrices. The role of the interface SiC polymer is suggested as the origin of the observed second order nonlinear optical susceptibility in the hybrid materials based on poly-(methylmethacrylate) (PMMA) or poly-(*N*-vinylcarbazole) matrices. In this work, we report an analysis of the electro-optical response of this hybrid system as a function of the ncSiC content and surface state in order to precise the interface effect in the observed phenomenon. Two specific ncSiC samples with similar morphology and different surface states are incorporated in the PMMA matrix. The effective Pockels parameters of the corresponding hybrid nanocomposites have been estimated up to 7.59 ± 0.74 pm/V (1 wt. % of ncSiC in the matrix). The interfacial region ncSiC polymer is found to play the main role in the observed effect. Particularly, the electronic defects on the ncSiC nanocrystal surface modify the interfacial electrical interactions between the two components. The results are interpreted and discussed on the basis of the strong influence of these active centers in the interfacial region at the nanoscale, which are found to monitor the local hyperpolarizabilities and the macroscopic nonlinear optical susceptibilities. This approach allows us to complete the description and understanding of the electro-optical response in the hybrid SiC/polymer systems.

DOI: 10.1103/PhysRevB.74.205417 PACS number(s): 81.07.Pr, 78.20.Jq, 42.65.An, 82.35.Np

I. INTRODUCTION

Due to their size-dependant physical properties, semiconducting nanocrystals are promising materials for a wide range of applications. Particularly, nanocrystals exhibit quantum confinement effect as well as modified electronic band structure. Specific linear and nonlinear optical properties are also expected and differ from those of the bulk material.[1,2] Moreover, the interface reconstruction and the chemical disorder at the particle surface play a crucial role at the nanometric scale, leading to enhanced interactions with the surrounding medium or between nanoparticles. In order to take advantage of these potential effects, an appropriate strategy is to combine semiconducting nanocrystals and organic/inorganic matrices. Particularly, hybrid nanocomposites based on polymer matrices and inorganic nanocrystals have been widely studied and developed.[3,4] Functional nanocomposites have been realized for various applications such as charge transport,[5] electro-[6] and photo-luminescence,[7] or photovoltaic cells.[8] In the field of nonlinear optics, hybrid materials incorporating organic or inorganic active chromophores are an alternative substitute to inorganic monocrystals, such as lithium niobate. The main reasons lie in the easy implementation and competitive performances for light modulation. Thus, second harmonic generation (SHG) and electro-optical (EO) activity are experimentally observed for a wide class of hybrid composites.[9,10] In a preliminary stage, silicon carbide nanocrystals (ncSiC) have been successfully associated with polymer matrices and an electro-optical modulation has been experimentally demonstrated.[11,12] The corresponding effective Pockels coefficients are comparable with those of bulk cubic 3C-SiC waveguides.[13] This methodology pointed out the potentialities of the hybrid systems based on SiC nanocrystals for the electro-optical modulation.

Our preliminary investigations focused on the first experimental demonstration of a local electro-optical effect associated with nonaligned ncSiC-doped poly-(*N*-vinylcarbazole) (PVK) matrices.[11] As a second step, the implementation of an efficient elaboration process of noncentrosymmetric hybrid films and the development of an adapted electro-optical set-up permitted to evaluate the EO response of poly-(methylmethacrylate) (PMMA) matrices incorporating ncSiC. The corresponding estimated linear and quadratic EO parameters, comparable to those associated with bulk SiC, evidenced the relevance of the hybrid system SiC/polymer as electro-optical modulator.[12] The interface SiC polymer was suggested as a key element in the observed phenomenon. However, significant mechanical contributions were also observed, mainly due to the sample holder configuration.

In this study, investigations of the linear EO effect in PMMA matrices incorporating SiC nanocrystals are carried out in order to clarify the origin of the enhanced nonlinear second order susceptibilities of the nanocomposites. In this aim, two specific ncSiC samples from similar morphology and presenting different chemical compositions and surface states have been incorporated in the reference PMMA matrix. The mechanical contributions, associated with the device configuration (sample holder), have been reduced in order to provide a better understanding of the relation between the surface properties of the nanoparticles and the EO response of the ncSiC/polymer composites without additional elasto-optical contributions. By varying the nanoparticle loading in the organic matrix and by considering the dispersion and surface state of the particular ncSiC samples in PMMA, this paper aims to clarify the influence of the interface ncSiC-polymer on the linear EO response of the hybrid system. Complementary measurements made on alternative polymer host matrices presenting various electrical activities and thermal properties compared to PMMA—namely the poly-(bisphenol-*A*-carbonate) (PC) and poly-(*N*-vinylcarbazole) (PVK)—will help to precise the origin of the observed effect.

The first part of this paper presents the elaboration process of the ncSiC/polymer nanocomposites. The different steps will be briefly presented, from the ncSiC synthesis by laser pyrolysis and the elaboration of thin hybrid films, to the final structure of the EO cell. The second part deals with the experimental setup used to probe the linear birefringence induced by Pockels effect and a definition of the linear EO parameters investigated will be presented. The relevant physical properties of the samples will be discussed in more details in Sec. III, to point out the particle surface features, which govern their dispersion in the precursor suspensions SiC/polymer/solvent and the interface with the polymer. Finally, the electro-optical investigations on the hybrid nanocomposites will be presented and a discussion will be developed to understand the role of the interface SiC/polymer on the nonlinear second order susceptibility revealed in the system.

II. EXPERIMENTAL SECTION

A. Elaboration of the hybrid SiC/polymer thin films

1. SiC nanocrystals synthesis

Because a control of the nanoparticle surface is crucial for the considered application, the ncSiC are synthesized by laser pyrolysis which permits a tuning of the nanocrystal properties through the synthesis conditions and post-annealing treatments. As previously described,[14,15] ncSiC nanocrystals are synthesized by laser pyrolysis of a gaseous mixture composed by silane (SiH_4) and acetylene (C_2H_2). Well-crystallized SiC nanoparticle samples are typically obtained with an average diameter that can be tuned between 10 to 100 nm depending on the synthesis parameters. As-formed powders are usually annealed at 1400 °C under argon for 1 h in order to improve their crystallinity and surface quality without a significant increase of their size.

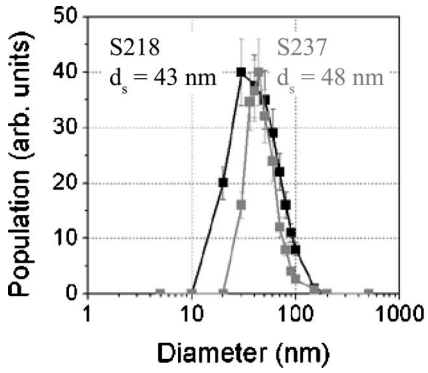

FIG. 1. Size distribution of a ncSiC(S218 and S237)/PMMA/Chloroform suspensions ($C_{PMMA/Chloroform}$=60 mg/ml; $C_{SiC/PMMA}$ =1 wt. %) after ultrasonic treatment. Isolated SiC nanoparticles with a mean diameter close to the B.E.T diameter of the dried nanopowders are evidenced.

2. Elaboration of the hybrid ncSiC/polymer nanocomposites thin films

(a) *Preparation of the initial precursor mixtures*. In a first step, the SiC nanoparticles are homogeneously dispersed in pure chloroform (0.02 to 0.12 wt. %) by using an ultrasonic stirring procedure. The dissolved polymer is then added to the solution, followed by an additional stirring step. The ncSiC content and polymer concentration, as well as the ultrasonic power and stirring time, are improved in order to obtain homogeneous suspensions of isolated nanoparticles without aggregation or sedimentation on a large time scale. The ncSiC content in suspension corresponds to a final concentration of ncSiC ranging between 0.5 and 2 wt. % with regard to the polymer (0.02 to 0.08 wt. % with regard to the solvent). Because the ncSiC dispersion in the polymer matrix is a crucial step, a rigorous control is performed on the suspensions SiC/polymer/chloroform by photon correlation spectroscopy or PCS (Malvern Zetasizer 1000HS). Considering the low particle content with regard to the solvent, this technique can indeed provide specific information on the populations of particles in the initial suspensions following the stirring procedure. The autocorrelation function of the light intensity scattered by the suspension is evaluated and adjusted to determine the translational diffusion coefficient D_i associated with the ith size class of nanoparticles in solution (see Ref. 16 for experimental and fitting procedure details). From this coefficient, the hydrodynamic diameters d_i of particles in solution are determined by using the Stokes-Einstein's law

$$d_i = \frac{kT}{6\pi\eta D_i},$$

where η is the viscosity of the polymer dissolved in chloroform and measured by capillary viscosimetry, k is the Boltzmann's constant, and T the temperature. Such an approach has been previously used to characterize the dispersion behavior of SiC nanoparticles in water.[16] Figure 1 presents the size distribution of SiC nanoparticles (S218 and S237) dispersed within PMMA in chloroform ($C_{PMMA/Chloroform}$

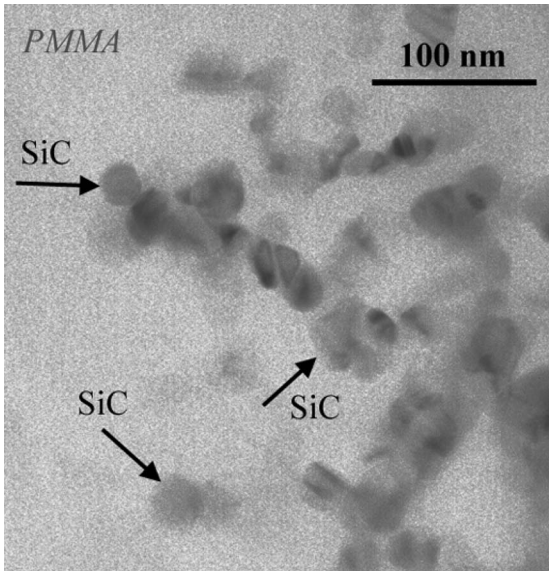

FIG. 2. Transmission electron micrograph showing the local dispersion of the ncSiC particles (S237) in the PMMA matrix (1 wt. % ncSiC loading).

=60 mg/ml; $C_{SiC/PMMA}$=1 wt. %). Nanoparticles with hydrodynamic diameters d_s close to the BET diameters of the dry nanopowders are evidenced in the suspensions. This observation is consistent with a monodispersed population corresponding to a majority of isolated SiC nanograins in the initial mixtures. It is worth noting that the PCS measurement gives an estimation of the mean hydrodynamic diameter of particles in solution (including the Stern and diffuse shells), which is then found slightly larger than the physical diameter of the nanograins. The error bars on d_s, induced by the fitting procedure and assuming that the particles are spherical, are evaluated at ±15%.[16] Finally, hybrid thin films are deposited by spin casting the SiC/polymer/chloroform suspensions onto ITO-coated (100 nm) glass substrate, previously cleaned. The spinning rate and suspension viscosities are improved for each polymer host in order to achieve films of good optical quality with a controlled thickness of 0.5 μm. The local dispersion of the ncSiC (S237) nanoparticles in the PMMA matrix is illustrated in Fig. 2 by a transmission electron micrograph. This latter was obtained by dispersing in ethanol a fraction of the scratched nanocomposite and depositing the preparation on a carbon grid. The particle distribution, mainly controlled by the homogeneity of the precursor suspension ncSiC/polymer/solvent, will be discussed hereafter.

(b) *Structuration of the hybrid thin films and poling procedure*. For the EO investigations, the samples are sandwiched by using a dielectric buffer layer (Teflon®, Goodfellow, France) and an ITO-coated glass as the top electrode (inset of Fig. 3). The buffer layer (10 μm thick) prevents short-circuits and parasitic conductivity through the hybrid active layer SiC/polymer during the poling process and the EO investigations. The final cell is 10 to 12 μm thick, with an investigated active area of 0.3 cm^2. All devices are annealed under primary vacuum (10^{-3} Torr) for 16 h in order to remove the solvent traces and to improve the film roughness and homogeneity. The annealing temperature is chosen near the glass transition temperature (T_g) of the polymer host matrix (T_g^{PMMA}=105 °C; T_g^{PC}=150 °C; T_g^{PVK}=190 °C). An additional electrical poling procedure is required to achieve the noncentrosymmetry, by aligning the microscopic dipolar

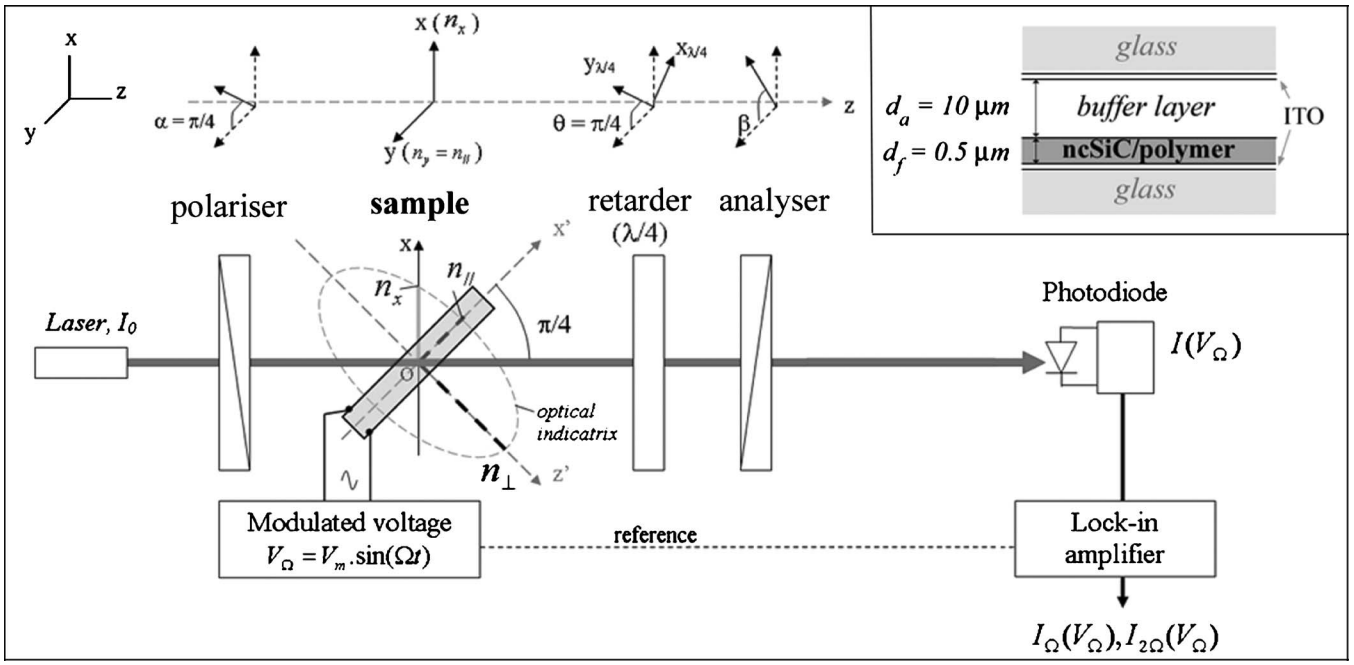

FIG. 3. Experimental setup used to probe the electro-optical birefringence in the SiC/polymer nanocomposite films. A modulated voltage is applied on the SiC/polymer thin films and the effective Pockels coefficient is estimated from the modulated transmitted intensities. The inset presents the SiC/polymer nanocomposite films sandwiched between ITO coated glass substrates separated by a dielectric buffer layer. This latter prevent shortcuts and parasitic currents during the application of poling (dc) and probing (ac) voltages.

centers in the isotropic polymer matrix. The standard procedure by electrodes was used by applying a static dc voltage (from 5 to 30 V/μm)for 30 min between the ITO electrodes of the devices after heating near T_g of the host matrix. The samples are then cooled at room temperature under applied electric field. The residual leak current was measured to be less than 10 μA during all the procedure.

B. Electro-optical setup

1. Effective Pockels coefficient

The poled hybrid thin films present the axial symmetry $C_{\infty v}$ with their optical axis (Oz') perpendicular to the substrate ($x'Oy'$ plane). Their optical properties are represented by the ordinary and extraordinary refractive indices $n_{\|}$ and $n_{\perp}$. When an external electric field E_i is applied on the devices, the optical indicatrix is perturbed by Pockels effect, represented by the effective Pockels coefficients r_{ijk}. The perturbed refractive indices can be expressed as

$$n'_{\|} = n_{\|} - \frac{n_{\|}^3 r_{11k}}{2} E_k$$

$$n'_{\perp} = n_{\perp} - \frac{n_{\perp}^3 r_{33k}}{2} E_k.$$

In this study, the EO effect is probed by applying a modulated voltage $V_\Omega = V_m \sin(\Omega t)$ between the two ITO electrodes of the devices, so that the only nonzero component of the corresponding electric field $E_3(\Omega) = E(\Omega)$ is oriented along the Oz' axis.

2. Experimental set-up

The electro-optical coefficients are measured by using an adapted Sénarmont-based setup.[12,17,18] The sample, located between polarizer, phase retarder and analyzer, is tilted at 45° with regard to the probing laser beam ($\lambda = 633$ nm, $P = 10$ mW) directed along the Oz axis of the laboratory frame (Fig. 3). With regard to the sample optical indicatrix and the incident polarization tilt ($\alpha = \pi/4$), the two optical modes in the sample propagate with different refractive indices n_x and n_y, function of the normal indices $n_{\|}$ and $n_{\perp}$. When the retarder is oriented with an angle $\theta = \pi/4$ with regard to the Ox axis, and under the modulated voltage V_Ω, the transmitted intensity can be expressed as a function of the analyser orientation (β) and the phase shift $\Gamma(V_\Omega)$ introduced by Pockels effect in the sample

$$I(\beta, \Gamma) = \frac{I_0 T_0}{2} [1 - \sin(\Gamma - 2\beta)]. \quad (1)$$

I_0 is the incident light intensity and T_0 the intrinsic transmission coefficient of the optical components including Fresnel losses. The angle β is fixed at the half-transmission point to ensure a linear regime under low modulated amplitude V_m, while compensating the natural birefringence $\Delta n^0 = n_x - n_y$ in the sample. The phase difference $\Gamma(V_\Omega)$ is then expressed as

$$\Gamma(V_\Omega) = \frac{2\pi L \Delta n'}{\lambda}$$

with

$$\Delta n' = n'_x - n'_y = \Delta n^0 + \frac{1}{2} n_{//}^3 r_e \frac{V_\Omega}{(d_a + d_f)}.$$

L is the optical path length in the active nanocomposite film of thickness d_f, d_a being the buffer layer thickness. The effective Pockels coefficient r_e is given by

$$r_e = r_{113} - \frac{n_x^3}{2 n_{//}^3} (r_{113} + r_{333}). \quad (2)$$

By using the Bessel expansion of expression (1), the transmitted modulated intensity $I_\Omega(V_m)$ detected by the lock-in amplifier is then limited in first approximation to the following expression:

$$I_\Omega(V_m) \approx \frac{I_0 T_0}{2} \frac{\pi L n_{//}^3 r_e}{\lambda (d_a + d_f)} V_m. \quad (3)$$

The experimental curves $I_\Omega(V_m)$ are linearly adjusted to determine the corresponding parameter r_e with accuracy less than ~10%. It is worth noting that the effective coefficient r_e defined in expression (2) includes the pure electro-optical effect, as well as the elasto-optical contributions (piezo-optics)

$$r^e_{ijk} = r^{EO}_{ijk} + r^{PZ}_{ijk}$$

with

$$r^{PZ}_{ijk} = - \frac{a^{(1)}_{ijpq} d_{kpq}}{n_{ip}^2 n_{qj}^2},$$

where $a^{(1)}_{ijkl}$ is the first order elasto-optic tensor and d_{ijk} the piezoelectric tensor. Moreover, large second order mechanical contributions (electrostriction and electrode attraction) were previously observed by measuring the quadratic electro-optic coefficient in the SiC/polymer nanocomposites.[12] However, these contributions were found sensitive to the sample configuration and the device holder geometry. A specific attention was paid to the constraints induced by the holder on the multilayer film glass-ITO/SiC-polymer/buffer/ITO glass. In this experimental approach, the sample geometry and holder configurations have been improved to reduce these mechanical contributions.

III. RESULTS AND DISCUSSION

A. Physical properties of the ncSiC samples

1. Morphology and chemical composition

In order to investigate the influence of the interface ncSiC-polymer in the observed EO phenomenon, two representative samples referred as S218 and S237 will be investigated hereafter. Both as-formed nanopowders have been annealed at 1400 °C under argon and specific area measurements by the B.E.T. method (Brunauer, Emmet, and Teller, on a Micromeritics Flowsorb II) lead to an estimation

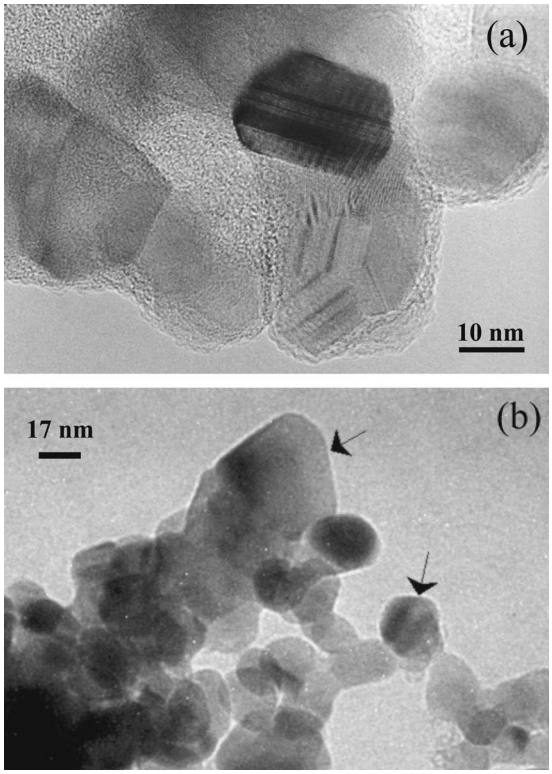

FIG. 4. Transmission electron microscopy picture (TEM) of the sample S218 (a) and S237 (b) annealed at 1400 °C (Ar). Well-defined SiC nanocrystals (~30 nm diameter) are found covered with an amorphous-like disordered layer for sample S218.

of the mean grain diameter of 40 nm for both annealed samples. Figure 4 presents the transmission electron microscopy pictures of S218 [Fig. 4(a)] and S237 [Fig. 4(b)] after annealing at 1400 °C. Sample S218 exhibits well-defined SiC nanocrystals (~30 nm diameter). The SiC crystalline core is found surrounded by a disordered or amorphous layer (a few nanometers thick), whose nature will be discussed hereafter. The sample S237 exhibits mainly spherical nanoparticles with a mean diameter in accordance with the B.E.T. estimation. A slight grain growth is visible on some particles and evidences of crystallisation are visible on this low magnification micrograph.

Samples S218 and S237 differ mainly by the chemical composition of the precursor mixture used during their synthesis. The atomic C/Si ratios, determined from elemental chemical analyzes, are evaluated to C/Si=0.87 for sample S218 and 1.02 for sample S237. It was shown that a deviation from the stochiometry leads to the presence of silicon-rich or carbon-rich disorderedlike phases at the particle surface.[19,20] This specificity can be revealed by Raman diffusion[20] or infrared absorption spectroscopy (Perkin-Elmer FTIR model 2000), here performed on cold pressed pellets of SiC particles mixed to KBr (Fig. 5). Beside the Si-C contribution being observed in both samples (700–970 cm^{-1}), S218 exhibits an additional absorption band in the range 1000–1250 cm^{-1}, attributed to Si-O bonds. The presence of Si-O-Si siloxane surface groups is evidenced by the contributions at 1100–1200 cm^{-1}, witness of a particle oxidation[21] in agreement with a silicon-rich phase in

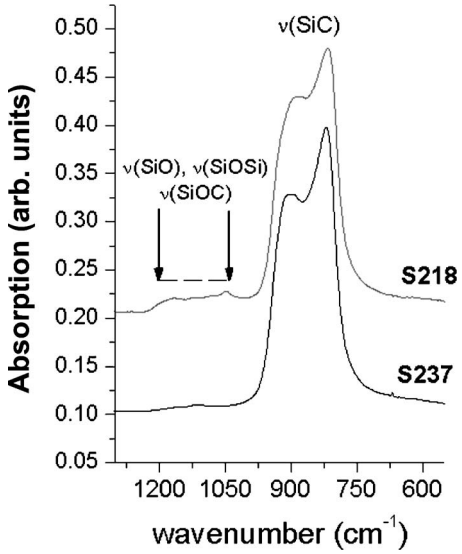

FIG. 5. IR absorption spectra of samples S218 and S237. Beside the Si-C bond contributions, the S218 gives rises to IR bands from Si-O and Si-O-C bonding in agreement with a strong reactivity of the silicon-rich surface shell with oxygen.

excess at the S218 nanoparticle surface. This observation is in agreement with the amorphous shell surrounding the crystalline SiC core evidenced by TEM, which could be assigned to the formation of an external silica layer upon oxidation. These contributions are not observed for sample S237.

2. Active electronic centers

Further information on the sample surface states can be acquired by paramagnetic electronic resonance, which provide information on the electronic centers or defects required for thermodynamic stabilization of the particle size and structure.[22] Both samples are characterized by the presence of different electronic active centers probed by electron paramagnetic resonance (EPR). They are hereafter referred as DI and DIV when involved in the sample S218, while DII and DIII coexist in the sample S237.[17] The sites DI and DII, which present anisotropic g tensors and isotropic hyperfine interactions, are associated with unpaired electrons interacting with four equivalent Si atoms in the SiC structure, in agreement with charged carbon vacancies (V_C). The site DIII (S237) is only observed for carbon-rich samples, and is associated with dangling bonds (DB) in isolated carbon phases, located at the outermost particle surface.[16] This assignment is in agreement with amorphous graphitic surface layers, as observed in disordered carbon arrangements.[23] Regarding the stability of the nanopowders, the external carbon-rich shells induce a relative inertia of sample S237 with respect to ambient conditions (oxidation). Unlike the site DIII, the site DIV (S218) is observed only in Si-rich samples and is specific to nanocrystalline silicon-rich phases, which are mainly located at the external surface of the SiC nanoparticles of sample S218, as seen by infrared absorption spectroscopy. This site DIV, which exhibits a high sensitivity to oxidation,[17] is responsible of a relative reactivity of the nanoparticle surfaces for sample S218 when exposed to partial

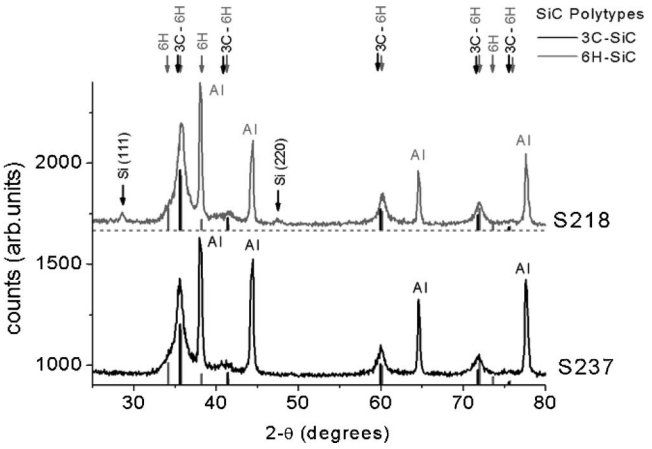

FIG. 6. X-Ray diffraction pattern of the as-formed nanopowders S218 and S237 on aluminium holder ($\lambda_{CuK\alpha 1}=1.54056$ Å). The contributions of both SiC polytypes 3C (cubic) and 6H (hexagonal) are evidenced for both samples.

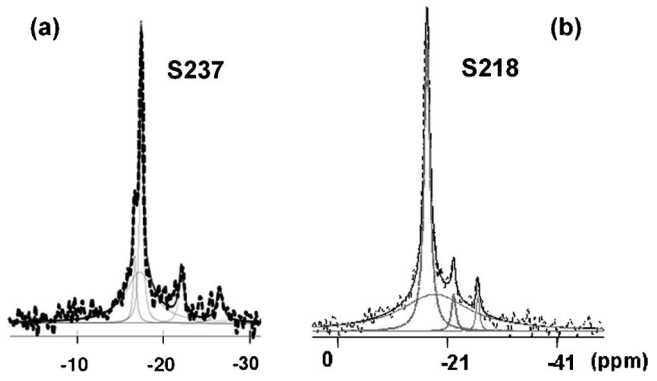

FIG. 7. Solid state nuclear magnetic resonance spectra (^{29}Si MAS-NMR) of samples S237 (a) and S218 (b) annealed at 1400 °C. The presence of both polytypes 3C and 6H-SiC is evidenced through the contributions at −14.6, −20.4, and −24.7 ppm. A amorphouslike SiC fraction is also revealed by the broad line centered at −18 ppm.

oxygen pressure or to ambient atmosphere. This observation is in agreement with the presence of silicon-rich phases at the particle surface for this sample.

3. Structural features

X-ray diffraction patterns of both samples are presented in Fig. 6. The observed features reveal diffraction line broadening due to nanoscale particles, and evidence the presence of the cubic 3C and hexagonal 6H-SiC polytypes for both samples. Particularly, the low intensity feature located at $2\theta=34.2°$ reveals the presence of the hexagonal 6H polytype for both samples. By a deconvolution of the first intense SiC diffraction line ($2\theta=35.6°$) with the two polytype contributions—assuming that the line broadening is mainly due to a size effect and by using the Scherrer relation—the crystallite mean diameter is evaluated at 25/28 nm for both samples, in accordance with the high resolution TEM observations [presented here on Fig. 4(a) for sample S218]. Sample S218 exhibits additional contributions at $2\theta=28°$ and 45.7° associated with a crystallized fraction of the silicon excess in the sample.

Further structural information can be deduced from the nuclear magnetic resonance (NMR) spectra given in Fig. 7 for both samples annealed at 1400 °C. Three mains contributions are evidenced in the ^{29}Si MAS-NMR spectra (−14.6, −20.4, and −24.7 ppm), associated with the presence of the 6H and 3C polytypes,[11,19] in similar relative proportions for both samples. An amorphous SiC fraction is also revealed for both samples through the wide contribution centered at −18 ppm. This latter, associated with the chemical disorder and reconstructed-surface at the nanoparticle boundaries, is found reduced by annealing the powders at 1400 °C.

Finally, the main features of the ncSiC samples used in this study—chemical composition, B.E.T. diameters, crystalline polytypes, and electronic centers—are summarized Table I. The two ncSiC samples present similar morphology and crystalline structure. They differ mainly through their surface properties and associated reactivity with regard to their environment. These specific features allow us to investigate the influence of the interface ncSiC-polymer on the hybrid nanocomposites EO response.

B. Electro-optical activity in ncSiC-based PMMA nanocomposites

The effect of the incorporation of SiC nanocrystals on the electro-optical response of the polymer nanocomposite is demonstrated by using the PMMA matrix incorporating 1 wt. % of S218. The modulated transmitted intensities $I_\Omega(V_m)$ have been measured for the as-prepared and SiC-loaded PMMA matrices. Both samples have been characterized with and without electrical poling under a static electric field of 15 V μm^{-1} around the polymer glass transition temperature (135 °C) for 30 min. From the experimental curves, the linear effective Pockels coefficients r_e are estimated according to Eq. (3) and summarized in Table II. The unpoled composites, as well as the poled PMMA matrix, exhibit low EO parameters (∼0.10–0.20 pm/V). However, the poled matrix incorporating the ncSiC S218 exhibits a Pockels coefficient of 5.11 pm/V, larger than those associated with crystalline SiC waveguides.[13] Moreover, this value is in the same order of magnitude than those of organic matrices doped with organic chromophores possessing large hyperpolarizabilities.[24] In the considered hybrid material, the high EO value evidences an enhancement of the quadratic

TABLE I. Main physical properties of the two ncSiC samples used in this study. The B.E.T. mean diameters are specified, as well as the crystallite sizes evaluated from the XRD diffraction patterns, and the corresponding crystalline structures. The electronic centers evidenced by EPR are also indicated.

	C/Si (atomic)	d_{BET} (nm)	d_{XRD} (nm)	SiC polytypes	Electronic sites	
					volume	*surface*
S218	0.87	40	25-28	6H and 3C	DI (V_C)	DIV
S237	1.02	40	25-28	6H and 3C	DII (V_C)	DIII

TABLE II. Experimental effective Pockels coefficient r_e of PMMA based matrices incorporating 1% SiC nanocrystals S218. The coefficients corresponding to unpoled and poled composites (135 °C-15 V/μm−30 min) are presented.

	r_e (pm/V)	
	unpoled	*poled*
PMMA	0.10±0.01	0.20±0.02
PMMA - 1 wt. % S218	0.11±0.02	5.11±0.49

nonlinear optical susceptibility of the poled composites by incorporating the SiC nanoparticles.

The poling procedure is therefore found necessary to achieve a significant macroscopic response of the nanocomposite. Let us consider the probability $p(\theta)$ that a local molecular dipole $\vec{\mu}$ is oriented at an angle θ with regards to the poling electric field $\vec{E}_p$

$$p(\theta) = p_0 e^{-\vec{\mu} f^0 \vec{E}_p / kT_p},$$

where f^0 is the Onsager's factor taking into account local corrections, k is the Boltzmann's constant, and T_p the poling temperature. The poling procedure is a requirement to maximize $p(\theta)$ and to achieve a macroscopic noncentrosymmetry in the nanocomposite through both the poling electric field $\vec{E}_p$ and the temperature T_p. Figure 8 presents the evolution of r_e versus the amplitude E_p and temperature T_p for sample S218 in PMMA, and allow us to evaluate the suitable poling parameters as E_p=15 V μm^{-1} and T_p=135 °C for this system. Under these conditions, both the electric field and the temperature are optimum to align the molecular dipolar centers through local reorganizations around the polymer chains, while avoiding strong dipole-dipole interactions. The origin and nature of these local dipoles will be discussed in the next parts.

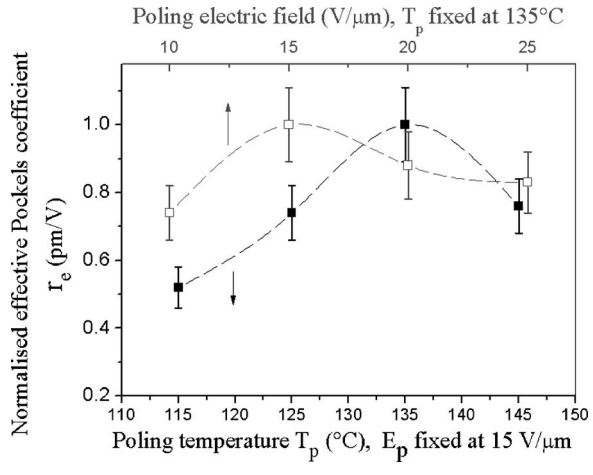

FIG. 8. Normalized effective Pockels coefficient of PMMA +1 wt. % S218 nanocomposite as a function of the poling parameters: Temperature T_p (at fixed electric field E_p=15 V/μm) and Electric field E_p (at fixed temperature T_p=135 °C).

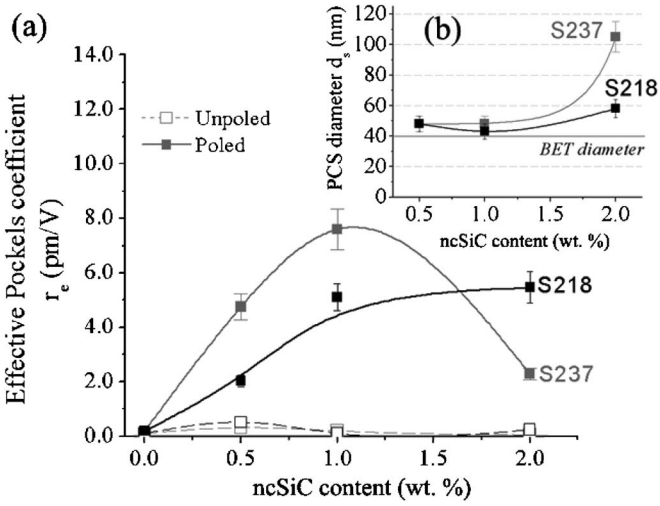

FIG. 9. (a) Effective Pockels coefficient r_e as a function of the ncSiC (S218 and S237) loading in the PMMA polymer matrix. (b) PCS mean particle diameter associated with the initial solution ncSiC/PMMA/Chloroform used to deposit the film by spin-coating. The B.E.T. diameter of the initial nanopowders is given for comparison.

C. Role of the SiC/polymer interface

Figure 9(a) presents the evolution of r_e for the PMMA matrices as a function of the ncSiC (S218 and S237) loading in the composite. An increase of the EO coefficient is evidenced as the ncSiC content increases for both samples (up to 5.11 and 7.59 pm/V for 1 wt. % of S218 and S237, respectively). This result is found in agreement with the influence of the ncSiC loading in the matrix on the EO response of the hybrid composites. At a higher ncSiC content (2 wt. %), both nanocomposites exhibit slightly different behaviors. The EO coefficient associated with the S218-doped PMMA matrix reaches a maximum value of 5.47 pm/V up to 2 wt. % of ncSiC in the matrix. At the opposite, higher particle content leads to a decrease of the electro-optical coefficient r_e down to 2.26 pm/V for a concentration of 2 wt. % in the S237-doped matrix. Although the EO effect is clearly correlated with the SiC loading in the matrix, it is necessary to consider the size distribution of the ncSiC in the PMMA matrix—or in the initial ncSiC/polymer/solvent mixture which controlled the morphology of the solid nanocomposite—for a better understanding of this tendency. Figure 9(b) presents the evolution of the PCS diameters d_s in the initial mixtures used to spin cast the hybrid films. For the ncSiC concentrations up to 1 wt. %, the mean particle diameter in the solutions d_s is found close to the B.E.T. diameter of the initial nanoparticles, both for sample S218 and S237 (39 nm and 40 nm, respectively). This result shows that the stirring process is efficient up to this content and the increase of r_e is directly linked with the increase of the SiC chromophore concentration. For a ncSiC content of 2 wt. %, the PCS measurements reveal a mean particle diameter d_s of 58 nm for sample S218 and 105 nm for sample S237 in solution with the PMMA. The nanoparticles are then not fully dispersed in the initial suspension previously to the spin-coating process, and larger

TABLE III. Effective electro-optical coefficients evaluated for unpoled and poled PMMA matrices incorporating 1 wt. % of SiC samples S218 and S237. The mean diameters of the initial nanopowders are given, as well as the mean particle diameters measured by PCS in the initial ncSiC/PMMA/chloroform suspensions.

	C/Si (atomic)	d_{BET} (nm)	d_s (PCS) (nm)	r_e (pm/V)	
				unpoled	*poled*
S218	0.87	40	43	0.11±0.02	5.11±0.49
S237	1.02	40	48	0.20±0.02	7.59±0.74

aggregates are formed in the solution based on S237. The decrease of r_e for this concentration can therefore be associated with a decrease of the interfacial area between the nanoparticles and the PMMA chains in the matrix. This result evidences the role of the interface ncSiC-polymer in the linear electro-optical response of the composites. Unlike S237, sample S218 presents better dispersion behavior up to 2 wt. % of particles with regard to the polymer. The apparent saturation of the EO coefficient for this concentration may arise from a slight agglomeration in the initial suspension, and/or higher dipole-dipole interactions. These couplings, due to a high particle density, tend to prevent an efficient alignment during the poling procedure. The next parts are devoted to a study of the influence of the nanoparticles surface state and polymer nature on the EO response of the composites.

D. Influence of the ncSiC surface state

The influence of the nanoparticles surface state can be determined by a comparison between the PMMA matrix incorporating 1 wt. % of S218 and S237 samples. Indeed, both samples exhibit a mean particle diameter around 40 nm and good dispersion properties in the initial blends SiC/PMMA/chloroform. However, the EO characterizations of the poled samples (E_p=15 V μm^{-1} and T_p=135 °C for 30 min) give an estimation of the effective Pockels coefficient r_e of 5.11 and 7.59 pm/V for samples S218 and S237, respectively (Table III). Both samples possessing similar dispersion behavior at 1 wt. % of ncSiC in the initial SiC-PMMA-chloroform suspensions, this difference can be explained from the influence of the nanoparticle surface states on the interaction with the polymer. With the presence of specific electronic defects associated with a silicon-rich particle surface, sample S218 reacts with oxygen in ambient conditions.[22] The presence of these active centers is also responsible of a natural tendency to disperse in polar solvents, as observed in water.[16] At the opposite, the carbon-rich amorphous phases that partially cover the SiC core of the S237 nanoparticles are associated with the presence of dangling bonds, whose reactivity is found limited with regard to ambient conditions.[20] The origin of a different EO response for the PMMA-based matrices can then be mainly attributed to the different surface features revealed in the samples S218 and S237. A theoretical justification of such behavior can be sketched from the Pockels tensor coefficients r_{ijk}. They are related to the interaction between the quasistatic electric field E applied on the sample and the second order susceptibility $\chi^{(2)}_{ijk}$ of the medium through

$$r_{ijk} = -\frac{1}{n_{ip}^2}\chi^{(2)}_{ipk}\frac{1}{n_{qj}^2},$$

n_{ij} corresponds to the refractive index at the optical frequency defined in the dielectric frame. The nonlinear susceptibility corresponds to the spatial averaging (denoted by the bra-ket notation) of microscopic contributions through the quadratic local hyperpolarizabilities β_{IJK} (the capital subscripts I, J, and K are defined in the microscopic frame of a molecular dipole $\vec{\mu}$)

$$\chi^{(2)}_{ijk} = N\langle\beta^*_{IJK}\rangle,$$

where N represents the density of molecular dipoles $\vec{\mu}$ in the medium and the index "*" refers to the local corrections. The present results suggest that the local hyperpolarizabilies enhancement originates in the interface region between the ncSiC and the polymer chains. This observation is in accordance with molecular dynamics and quantum chemistry calculations on SiC clusters in a PMMA surrounding, which shows that β_{IJK} of the PMMA matrix are enhanced by the incorporation of the SiC clusters.[25] This effect was found linked to the existence of larger electric gradients at the SiC/polymer interfaces, by a contribution of the polymer chains to the local electric field seen by the ncSiC. The presence of dangling bonds in the carbon-rich phases on the nanoparticles surface (S237) is plausibly at the origin of a strong enhancement of the local hyperpolarizabilities. At the opposite, a relative passivation of the silicon-rich S218 particle surface by oxidation[26] could decrease these interactions once incorporated in the polymer matrix. These results point out the effect of the interfacial hyperpolarizabilities on the observed phenomenon.

E. Influence of the polymer matrix

To study the influence of the polymer on the EO response of the composites, two alternative polymers – PC and PVK – have been investigated and compare to the PMMA matrix. Prior to their deposition, the initial suspensions S218/polymer/cholroform present a homogeneous dispersion for the three different polymers, associated with a PCS diameter d_s close to the ncSiC particle diameter of S218. The three nanocomposites have been poled under a poling electric field of E_p=15 V μm^{-1} applied for 30 min, and by using optimized poling temperature with regard to the glass transition temperatures of the matrices (T_p^{PMMA}=135 °C, T_P^{PC}=160 °C, and T_P^{PVK}=190 °C). Figure 10 reports the corresponding effective Pockels coefficient r_e for the three S218-based composites (1 wt. %). The higher EO response is found for the PC matrix (7.42 pm/V), followed by the PMMA reference matrix (5.11 pm/V). The PVK matrix leads to a smaller EO parameter of 1.14 pm/V. An explanation of this behavior lies in the different chemical nature of the three polymers. The PC and PMMA polymers possess a polar group C=O which exhibits high polarizability. The lo-

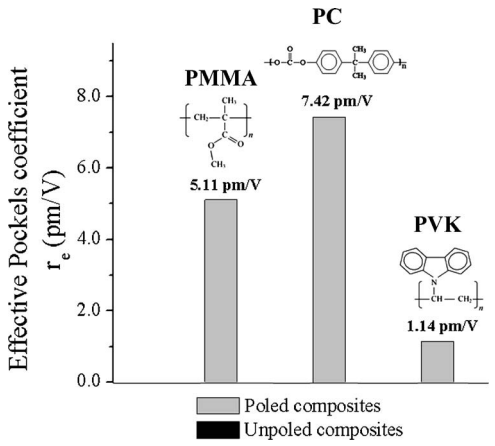

FIG. 10. Effective Pockels coefficient r_e as a function of the polymer nature (PMMA, PC, and PVK) for sample S218 (1 wt. %).

cal interaction with the dispersed SiC nanoparticles enhances the molecular dipoles and then the second order nonlinear susceptibility $\chi^{(2)}_{ijk}$. With a similar chemical structure than PMMA, the observation of a higher response for the PC matrix can be understood through its thermal properties. With a glass transition temperature $T_g^{PC}=150$ °C, the relaxation of the dipolar orientation in the PC matrix is slower at room temperature than for the PMMA matrix ($T_g^{PMMA}=105$ °C). The higher thermal stability of the PC matrix can then explain the higher EO response of the composites based on this polymer. At the opposite, PVK is a photoconductive polymer, since electrons associated with the carbazole group can be delocalized in the polymer backbone under light irradiation. A local spreading of the electronic density could then lower the interfacial polarization effects, leading to smaller Pockels coefficients. It is worth noting that these tendencies are observed for sample S237 as well (not presented here). Thus, the experimental observations presented in this work demonstrate the role played by the interface ncSiC-polymer in the linear EO properties of the hybrid nanocomposites.

F. Time evolution of the EO response

Finally, the time evolution of the EO response was investigated on sample S237 incorporated in the PMMA matrix (1 wt. %). Figure 11 reports the evolution of the Pockels coefficient r_e versus time. A good stability of the EO response is evidenced, with a relative decrease of r_e around 20% after 600 h (25 days). A single exponential decay was used to adjust the curve, and the corresponding relaxation time was estimated to be at least ten times larger than in PMMA-based matrix incorporating organic push-pull molecules.[27] The long time stability of the hybrid system SiC/polymer could be understood through an improvement of the nanocomposite thermal properties by the incorporation of the inorganic ncSiC chromophores. However, further studies are required, especially at shorter time-scales (<1 s), to discriminate the origin of the relaxation process in this system.

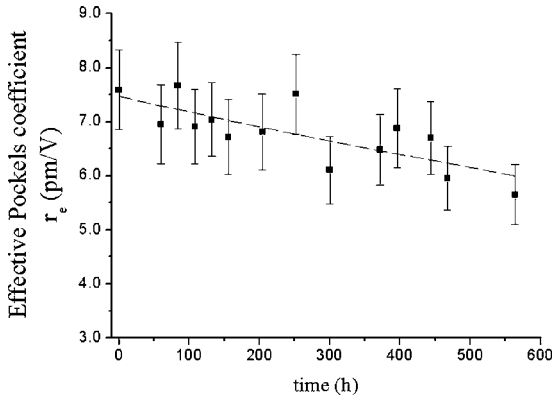

FIG. 11. Time evolution of the effective Pockels coefficient r_e for the sample S237 (1 wt. %) incorporated in the PMMA matrix.

IV. CONCLUSION

This work completes the analysis of all the process steps which lead to electro-optical active nanostructured hybrid materials based on wide band gap semiconducting nanoparticles (SiC) and polymer host matrices (mainly PMMA). The elaboration process has been improved and the sample configuration adapted to the electro-optical setup in order to limit the mechanical contributions in the measured linear effective Pockels coefficient. The aim of this study was to gain more insight about the physical origin of the electro-optical phenomena in the hybrid SiC/polymer system. By using complementary techniques (EPR, NMR, XRD, IR, etc.), the main features of the nanocomposites were revealed, thus allowing us to investigate the influence of the local interface SiC-polymer on the EO properties. We found that the main factors which control the EO response of the nanocomposites originate from the outermost nanocrystalline surfaces (structure, composition, active electronic centers) and depend on the polymer nature (polarization, thermal properties, etc.). Additionally, by incorporating results from numerical simulations extensively applied on these hybrid system from atomistic approaches,[25] a consistent interpretation is proposed regarding the observed EO response. The origins of both the macroscopic parameters (Pockels coefficients) and the microscopic local second order hyperpolarizabilities were discussed. The local polarizabilities at the origin of the phenomenon are involved intrinsically in the nanoparticle core and extrinsically from the interfaces. The surrounding polymer and the particle surface states are then found to enhance or overcome the EO phenomena, depending on their identified physical parameters. The main points of this interpretation, supported by the experimental measurement of the corresponding Pockels coefficients (r_e), can be summarized hereafter:

(1) The evaluated Pockels parameters reveal an enhancement of the EO properties of a PMMA matrix with the incorporation of SiC nanocrystals. Through the improvement of the ncSiC dispersion in the matrix, controlled by photon correlation spectroscopy on the initial mixtures ncSiC/PMMA/solvent, a maximum value of $r_e=7.59\pm0.74$ pm/V has been estimated for a PMMA matrix incorporating 1 wt. % of ncSiC nanoparticles. This value is

found larger than in crystalline SiC waveguides and in the same order of magnitude than those associated with all-organic guest-host systems.

(2) The combination of suitable experimental techniques used to determine the specific properties of the nanocomposites, allowed us to attribute the EO behavior as due to the interface regions between the dispersed ncSiC and polymer chains. In particular, by investigating nanoparticles with different surface states and compositions, the effects of nanoparticle surface reactivity and electronic defects on the EO response were determined in this work. The quadratic hyperpolarizabilities, at the origin of the probed nonlinear macroscopic susceptibility, are caused by these particular ncSiC surface features, as well as by the polymer nature.

However, although the cell geometry is improved in order to minimise the elasto-optical contributions, these latter remain involved in the effective EO response of the hybrid composites. A definitive conclusion on the potential use of these composites for light modulation requires a precise evaluation of the ratio between elasto-optical and true electro-optical contributions.

ACKNOWLEDGMENTS

This work has benefited from the financial supports of the "Région Pays de La Loire"- France under the programme (C.E.R Matériaux A Propriétés Spécifiques 2000-2006) and from the Research collaborative programs France-Poland and France-Ukraine (POLONIUM and DNIPRO 2005-2006, PAI).

*Corresponding authors. Electronic addresses:
johann_boucle@yahoo.fr and abdelhadi.kassiba@univ-lemans.fr

[1] A. P. Alivisatos, Science **271**, 933 (1996).
[2] L. Pavesi, L. Dal Negro, C. Mazzoleni, G. Franzo, and F. Priolo, Nature (London) **408**, 440 (2000).
[3] R. W. Boyd, R. J. Gehr, G. L. Fisher, and J. E. Sipee, Pure Appl. Opt. **5**, 505 (1996).
[4] G. D. Stucky, Nature (London) **410**, 885 (2001).
[5] Y. Wang and N. Herron, J. Lumin. **70**, 48 (1996).
[6] V. L. Colvin, M. C. Schlamp, and A. P. Alivisatos, Nature (London) **370**, 354 (1994).
[7] M. Tamborra, M. Striccoli, R. Comparelli, M. L. Curri, A. Petrella, and A. Agostiano, Nanotechnology **15**, S240 (2004).
[8] P. Ravirajana, S. A. Haque, J. R. Durrant, D. Poplavskyy, D. D. C. Bradley, and J. Nelson, J. Appl. Phys. **95**, 1473 (2004).
[9] J. Guo, J. Si, G. Qian, J. Qiu, M. Wang, and K. Hirao, Chem. Phys. Lett. **381**, 677 (2003).
[10] A. H. Yuwono, X. Junmin, J. Wang, H. I. Elim, J. Wei, L. Ying, and T. J. White, J. Mater. Chem. **13**, 1475 (2003).
[11] J. Bouclé, A. Kassiba, J. Emery, I. V. Kityk, M. Makowska-Janusik, J. Sanetra, N. Herlin-Boime, and M. Mayne, Phys. Lett. A **302**, 196 (2002).
[12] J. Bouclé, A. Kassiba, M. Makowska-Janusik, J. Sanetra, N. Herlin-Boime, A. Bulou, and S. Kodjikian, Opt. Commun. **246**, 415 (2005).
[13] X. Tang, K. G. Irvine, D. Zhang, and M. G. Spencer, Appl. Phys. Lett. **59**, 1938 (1991).
[14] M. Cauchetier, O. Croix, M. Luce, M. Michon, J. Paris, and S. Tistchenko, Ceram. Int. **13**, 13 (1987).
[15] N. Herlin-Boime, J. Vincens, C. Dufour, F. Ténégal, C. Reynaud, and R. Rizk, J. Nanopart. Res. **6**, 63 (2004).
[16] J. Bouclé, N. Herlin-Boime, and A. Kassiba, J. Nanopart. Res. **7**, 275 (2005).
[17] M. Aillerie, N. Theofanous, and M. D. Fontana, Appl. Phys. B **70**, 317 (2000).
[18] N. G. Theofanous, M. A. Ahmed, and G. Alexakis, Opt. Quantum Electron. **21**, 363 (1989).
[19] S. Charpentier, A. Kassiba, A. Bulou, M. Monthioux, and M. Cauchetier, Eur. Phys. J.: Appl. Phys. **8**, 111 (1999).
[20] A. Kassiba, M. Makowska-Janusik, J. Bouclé, J-F. Bardeau, A. Bulou, N. Herlin, M. Mayne, and X. Armand, Diamond Relat. Mater. **11**, 1243 (2002).
[21] G. Ramis, P. Quintard, M. Cauchetier, G. Busca, and V. Lorenzilli, J. Am. Ceram. Soc. **72**, 1692 (1989).
[22] S. Charpentier, A. Kassiba, J. Emery, and M. Cauchetier, J. Phys.: Condens. Matter **11**, 4887 (1999).
[23] R. C. Barklie, Diamond Relat. Mater. **10**, 174 (2001).
[24] D. Anestopoulos, G. Tsigaridas, P. Persephonis, V. Giannetas, I. Spiliopoulos, P. Karastatiris, and J. Mikroyannidis, Chem. Phys. Lett. **390**, 98 (2004).
[25] M. Makowska-Janusik, A. Kassiba, G. Failleau, and J. Bouclé (Materials Science, Poland, 1966, in press).
[26] A. Kassiba, M. Makowska-Janusik, J. Bouclé, J-F. Bardeau, A. Bulou, and N. Herlin-Boime, Phys. Rev. B **66**, 155317 (2002).
[27] K. D. Singer and L. A. King, J. Appl. Phys. **70**, 3251 (1991).